Human plasma proteome association and cytotoxicity of nano-graphene oxide grafted with stealth polyethylene glycol and poly(2-ethyl-2-oxazoline)

Miaoyi Wang,[†] Ove J. R. Gustafsson,[¶,≈] Ghizal Siddiqui,[‡,≈] Ibrahim Javed,[†] Hannah G. Kelly[‖,Π] Thomas Blin,[†] Hong Yin,[ʃ] Stephen J. Kent,[‖,Π,◊] Darren J. Creek,[‡] Kristian Kempe,[†] Pu Chun Ke[†*] and Thomas P. Davis[†,§*]*

[†] ARC Centre of Excellence in Convergent Bio-Nano Science and Technology, Monash Institute of Pharmaceutical Sciences, Monash University, 381 Royal Parade, Parkville, VIC 3052, Australia

[¶] ARC Centre of Excellence in Convergent Bio-Nano Science and Technology, Future Industries Institute, University of South Australia, University Boulevard, Mawson Lakes, SA 5095, Australia

[‡] Monash Institute of Pharmaceutical Sciences, Monash University, 381 Royal Parade, Parkville, VIC 3052, Australia

[‖] ARC Centre of Excellence in Convergent Bio-Nano Science and Technology, The University of Melbourne, Melbourne, VIC 3000, Australia

[Π] Department of Microbiology and Immunology, Peter Doherty Institute for Infection and Immunity, The University of Melbourne, Melbourne, VIC 3000, Australia

[◊] Melbourne Sexual Health Centre and Department of Infectious Diseases, Alfred Health, Central Clinical School, Monash University, Melbourne, Australia

[ʃ] CSIRO Manufacturing, Bayview Avenue, Clayton, VIC 3168, Australia

[§] Department of Chemistry, University of Warwick, Gibbet Hill, Coventry, CV4 7AL, United Kingdom

Email: thomas.p.davis@monash.edu; kristian.kempe@monash.edu; pu-chun.ke@monash.edu

[≈] These authors contributed equally to the presented work.

KEYWORDS: nano-graphene oxide, PEG, PEtOx, proteomics, protein corona

ABSTRACT

Polyethylene glycol (PEG) is a gold standard against protein fouling. However, recent studies have revealed surprising adverse effects of PEG, namely its immunogenicity and shortened bio-circulation upon repeated dosing. This highlights a crucial need to further examine 'stealth' polymers for controlling the protein 'corona', a new challenge in nanomedicine and bionanotechnology. Poly(2-ethyl-2-oxazoline) (PEtOx) is another primary form of stealth polymer that, despite its excellent hydrophilicity and biocompatibility, has found considerably less applications compared with PEG. Herein, we performed label-free proteomics to compare the associations of linear PEG- and PEtOx-grafted nano-graphene oxide (nGO) sheets with human plasma proteins, complemented by cytotoxicity and haemolysis assays to compare the cellular interactions of these polymers. Our data revealed that nGO-PEG enriched apolipoproteins, while nGO-PEtOx displayed a preferred binding with pro-angiogenic and structural proteins, despite high similarities in their respective top-10 enriched proteins. In addition, nGO-PEG and nGO-PEtOx exhibited similar levels of enrichment of complement proteins. Both PEG and PEtOx markedly reduced nGO toxicity to HEK 293 cells while mitigating nGO haemolysis. This study provides the first detailed profile of the human plasma protein corona associated with PEtOx-grafted nanomaterials and, in light of the distinctions of PEtOx in chemical adaptability, *in vivo* clearance and immunogenicity, validates the use of PEtOx as a viable stealth alternative to PEG for nanomedicines and bionanotechnologies.

INTRODUCTION

The rapid development of functional nanomaterials has enabled many advances in diagnostics, bioimaging and drug delivery in the past decades.[1, 2] Nanoparticles (NPs) grafted with specific polymers such as polyethylene glycol (PEG) become suspended in the aqueous phase and biocompatible. PEGylation also discourages protein fouling as the polymer layer acts as an entropic spring to fend off the surface adsorption of biomolecules. Collectively, these features have consolidated PEGylation as a 'gold standard' for surface functionalization in biomedical and engineering applications.[3]

It is well established that NPs readily adsorb a 'corona'[4-7] of proteins upon introduction into a biological milieu, a phenomenon resulting from hydrophobic, electrostatic and van der Waals interactions as well as hydrogen bonding between the NPs and proteins in the fluid environment. The transformation from bare NPs to NP-protein complexes usually confers the NPs with improved suspendability and a new biological identity that drives *in vivo* interactions and clearance of the NPs.[8, 9] Binding with NPs could also impact the conformation of adsorbed proteins, thereby inducing exposure of new epitopes and potentially altering protein function. For example, activated phagocyte recognition of a protein corona via enriched complement components may lead to decreased systemic retention for a particular NP,[10, 11] a characteristic undesirable for drug delivery. Accordingly, surface functionalization to incorporate 'stealth' polymers is a logical solution to minimize and control the protein corona for effective design and targeted delivery of nanomedicines.[12]

PEG is by far the most commonly used polymer for creating 'stealth' NPs. However, PEG is not biodegradable and the *in vivo* accumulation of PEGylated therapeutics can cause the production of anti-PEG antibodies to accelerate blood clearance and severe hypersensitivity reactions following administration.[3, 13-18] In addition, the heavily crowded patent landscape of PEG has also triggered intensive search for alternative stealth polymers.[19-21]

Poly(2-oxazoline)s (POx) are an emerging class of polymers,[22] which provide access to highly functional polymers with tuneable properties simply by changing their side chain.[23, 24] The possibility to introduce functional groups at the α-, and ω-polymer chain ends and, contrary to PEG, in the side chains makes POx available for a wide range of post-polymerization modifications,[23, 25] which can be exploited, e.g. for high drug loadings in polymer-drug conjugates.[26] In particular, the short homologues poly(2-methyl-2-oxazoline) (PMeOx) and poly(2-ethyl-2-oxazoline) (PEtOx) have been demonstrated to be valuable alternatives to PEG with similar water-solubility, biocompatibility and stealth/protein repellent properties.[27] Moreover, PMeOx and PEtOx offer potential benefits over PEG, including (i) relatively low viscosities of their aqueous solutions, (ii) depending on molecular mass, they can be excreted in urine and have so far yet to show accumulations in organs, and (iii) they are considered non-immunogenic and to date no POx-antibodies in human populations have been reported.[28] In terms of their interaction with proteins, limited studies performed with full serum have only looked into the mass deposition of proteins rather than the detailed composition of protein corona.[29, 30] One recent study has examined the antifouling capacity of poly(organosiloxane) (POS) NPs grafted with linear PEG and PEtOx exposed to fetal calf serum.[31] However, an in-depth comparison of the stealth performance and protein corona profile of PEtOx versus PEG against human plasma proteins remains lacking despite the large number of studies into POx-based particles for biomedical applications and the high relevance of such data for the development of nanomedicine and bionanotechnology.[32] Furthermore, research on the protein corona has almost exclusively adopted spherical or cylindrical NPs, overlooking the importance of NP shape in determining corona formation. Nano-graphene oxide (nGO), specifically, is a one-atom thin, 2D nanomaterial with small lateral dimensions and a large surface area. nGO possesses exceptional electronic, photothermal and mechanical properties and has found many biomedical applications.[33-39] Here we detail the human plasma protein association of a novel nanomaterial, PEtOx-grafted nGO (nGO-PEtOx), in comparison with that of PEG-grafted nGO (nGO-PEG). Liquid chromatography coupled to mass spectrometry (LC-MS/MS) was used post synthesis for label-free quantitation (LFQ) of proteins

present in the NP protein coronas. Although both nGO-PEG and nGO-PEtOx exhibited superior antifouling compared to bare nGO, they were each associated with different subsets of plasma proteins essential to major physiological functions. In addition to the comparable corona profiles observed for high abundance opsonins, there was a significant enrichment of apolipoproteins (*APOA1/A2/C1/A4/H, CLU*) for nGO-PEG, and pro-angiogenic, structural and acute-phase plasma proteins for nGO-PEtOx, respectively. Together, this study provides the first report on the unique corona proteome in human plasma and *in vitro* toxicity profiles of nGO-PEG and nGO-PEtOx, implicating PEtOx as a viable stealth polymer alternative to PEG for biomedical and biotechnological applications.

MATERIALS AND METHODS

Materials

A nano-graphene oxide (nGO, ~50×100 nm in lateral dimensions) suspension was obtained from Sigma-Aldrich. PEG and PEtOx polymers with amine end groups (MW: 2,000 g/mol) were synthesized according to protocols described previously.[40, 41] The polymers were designed to have the same molecular weight in order to minimize any size-induced variability. All other chemicals were obtained from Sigma-Aldrich and used as received unless otherwise specified.

NMR spectroscopy

Nuclear magnetic resonance (NMR) spectra were recorded using a Bruker UltraShield 400 spectrometer running Bruker Topspin, version 1.3 and operating at 400.13 MHz for ^{1}H. Deuterated chloroform (CDCl$_3$) was used as solvent. Chemical shifts were recorded in parts per million (ppm), referenced to residual solvent frequency ^{1}H NMR: CDCl$_3$ = 7.26.

Size exclusion chromatography

DMAc size exclusion chromatography (SEC) was performed using a Shimazu modular system consisting of a SIL20AD automatic injector, a DGU12A degasser, a CTO10A column oven, a

LC10AT pump, a RID10A differential refractive-index detector, and a SPD10A Shimadzu UV/Vis detector. A 50×7.8 mm guard column followed by three KF-805L columns in series (300×8 mm linear columns, bead size: 10 μm, pore size: 5,000 Å maximum) were used for the analyses. *N,N'*-Dimethylacetamide (DMAc, HPLC grade, 0.03% w/v LiBr) with a flow rate of 1 mL/min and a constant temperature of 50 °C was used as the mobile phase. The samples were filtered through 0.45 μm filters prior to injection. The instrument was calibrated using commercially available linear polystyrene standards (0.5-2,000 kDa, Polymer Laboratories). Chromatograms were processed using Cirrus 2.0 software (Polymer Laboratories).

nGO functionalization procedures

nGO (2 mg/mL) was treated with probe sonication for 5 min in an ice bath to ensure its dispersity. The first step of the reaction was to convert the OH groups on the nGO surface to –COOH groups via conjugation of acetic acid moieties. NaOH (2.4 g) and chloroacetic acid (2.0 g) were added to the nGO aqueous suspension (10 mL) and bath-sonicated for 5 h. This step functionalized nGO by carboxylation. The carboxylated nGO suspension was then neutralized by repeated washing with Milli-Q water through centrifugation (supernatant was removed after each centrifugation cycle). Eppendorf centrifuge 5804 was used and set for 10 min and 16,300 *g* for each washing cycle. Purified carboxylated nGO was then diluted with Milli-Q water to an optical density of 0.4 at 808 nm. Then a solution of linear PEG or PEtOx with an amine end group (10 mg/mL) was added to the diluted carboxylated nGO suspension and the mixture was bath-sonicated for 10 min. Next, *N*-(3-dimethylaminopropyl)-*N'*-ethylcarbodiimide hydrochloride (EDC) was added to make the final EDC concentration of 10 mM. The mixture was stirred at room temperature for 24 h, and the reaction was terminated by β-mercaptoethanol (50 mM). The mixture was dialyzed in Milli-Q water for 12 h and then centrifuged at 16,300 *g* for 30 min to obtain pure nGO-PEG and nGO-PEtOx from the pellets. nGO-PEG and nGO-PEtOx were re-dispersed in Milli-Q water for further use. The concentrations of nGO-PEG and nGO-PEtOx were determined by lyophilization. The grafting density of PEG and PEtOx polymers was calculated to be ~0.18 and 0.16 polymer chains/nm^2, respectively, according to

percentage weight losses of the polymers obtained by thermogravimetric analysis (TGA) and the physical dimensions of the nGO (50×100 nm, double-sided polymer grafting).

Thermogravimetric analysis

Thermogravimetric analysis (TGA) measurement was implemented using a PerkinElmer Pyris 1 TGA and Pyris 1 software measuring at a rate of 20 °C/min from 100 °C to 700 °C (hold at 100 °C for 1 min to eliminate water).

Dynamic light scattering and zeta potential

The hydrodynamic sizes and zeta potentials of the nGO suspensions (at 0.1 mg/mL in Milli-Q water) were acquired at room temperature using a dynamic light scattering device (Zetasizer Nano ZS, Malvern Instruments) with Zeta software 7.03, refractive index 1.33, absorption 0.010, viscosity 0.8872 cP, temperature 25 °C, and equilibration time 120 s. DTS-1070 cells were used for measurements at a backscattered angle of 173° and a wavelength of 633 nm. The measurements were carried out for each sample in triplicate, using folded capillary zeta cells.

Transmission electron microscopy and energy-dispersive X-ray spectroscopy

nGO (bare nGO , nGO-PEG and nGO-PEtOx) suspensions at a concentration of 0.1 mg/mL were pipetted onto glow discharged (15 s) 400 mesh copper grids (Formvar film, ProSciTech) and allowed 60 s of adsorption. Excess solution volume was drawn off using filter paper and the grids were washed twice using Milli-Q water, with excess removed. The grids were stained with 1% uranyl acetate for 30 s and excess stain drawn off. The grids were completely air-dried. High resolution imaging and EDX elemental analysis were performed on a Tecnai G2 F20 transmission electron microscope (FEI, Eindhoven, Netherlands) operating at 200 kV. The experiment was repeated three times.

Infrared spectroscopy

Attenuated total reflectance-Fourier transform infrared (ATR-FTIR) spectra were generated using a Shimadzu IRTracer 100 FTIR spectrometer with a GladiATR 10 single reflection ATR accessory.

The spectra were acquired in the mid-infrared region of 4,000-800 cm^{-1} at resolution of 8 cm^{-1} (512 scans) and analyzed by LabSolution IR software.

Raman spectroscopy

Raman spectra were acquired using an inVia confocal Raman microscope (Renishaw). The three types of nGO (bare, nGO-PEG- and nGO-PEtOx) with or without plasma protein coatings, as well as the plasma protein control in aqueous solution (0.5 mg/mL), were mounted on microscope slides and air-dried. The dried samples were excited by a laser line at 785 nm, with a power of 500 mW. Spectra were stored with in-built WiRE 2.0 software.

Collection and processing of healthy donor human plasma proteins

Details of the method are described in a previous publication.[21] Blood was collected from three different healthy donors after obtaining informed consent for any experimentation in this study, in accordance with the University of Melbourne Human ethics approval 1443420 and the Australian National Health and Medical Research Council Statement on Ethical Conduct in Human Research. All experiments were performed in compliance with the relevant laws and institutional guidelines of Monash University Occupational Health & Safety. The proteomic experiments and follow-up analysis were done using the plasma from the three donors to ensure robust results. The analysis of the abundance of coronal proteins was performed by taking average of the three replicates, and only those that were statistically significant were presented.

Corona formation and isolation

Bare, PEG- and PEtOx-grafted nGO (1 mg/mL) in 10 mM phosphate-buffered saline (PBS) were mixed with plasma proteins to make a final concentration of 0.2 mg/mL in 1 mL suspension. The nGO-plasma mixtures were incubated at 37 °C for 24 h to obtain hard protein coronae. The samples were then centrifuged at 16,300 g for 15 min at room temperature to isolate nGO-'hard' protein corona complexes from the remaining plasma, a common methodology in the field. The supernatant was completely removed and the nGO-protein corona pellets were washed 3× with 10 mM fresh PBS.

Following the washes, 50 µL of 5% β-mercaptoethanol (Sigma-Aldrich) in a 4× reducing loading dye (240mM Tris, pH 6.8, 8% SDS, 40% glycerol, 0.04% (w/v) bromophenol blue) was added to each nGO sample and incubated at 95 °C for 5 min. The nGO samples were pelleted by centrifugation for 3 min at 21,100 g at 4 °C, and the supernatants (20 µL) of each sample were resolved on a pre-cast 1D PAGE gel (Mini-PROTEAN® TGXTM, Bio-Rad Laboratories) using 1× mix of a 10× premixed electrophoresis buffer (25 mM Tris, 192 mM glycine, 0.1% SDS, pH 8.3, BioRad) at 200 V/0.04 A/8 W for 5 min. The gel was incubated in Instant Blue stain (Expedion Ltd) for 30 min on a shaker to fix and visualize the protein bands. Milli-Q water was then used to de-stain the gel for 1 h (fresh Milli-Q water every 20 min) prior to further processing.

In-gel proteolytic digestion, plasma control sample preparation, LC-MS/MS analysis and label-free quantification

The entire region of the gel containing resolved proteins was excised and subjected to an in-gel trypsin digestion procedure, as described previously.[21] Briefly, peptides were extracted, dried in a Speed-Vac, and stored at -20 °C until analysis. On the day of analysis, samples were reconsituted in 20 µL of 2% acetonitrile (ACN), 0.1% formic acid and LC-MS/MS analysis with data-dependent acquisition was carried out as previously described with minor modifications.[42] Reconsituted samples were loaded at a flow rate of 15 µL/min onto a reversed-phase trap column (100 µm × 2 cm), Acclaim PepMap media (Dionex), which was maintained at a temperature of 40 °C . Peptides were then eluted from the trap column at a flow rate of 0.25 µL/min through a reversed-phase capillary column (75 µm × 50 cm) (LC Packings, Dionex). For label-free proteomic analysis, the HPLC gradient was set to 98 min using a gradient that reached 30% ACN after 63 min, 34% after 66 min, 79.2% after 71 min for 6 min, following which there was an equilibration phase of 20 min at 2% ACN. Peptide sequences (and protein identity) were determined using MaxQuant software (version 1.6.0.1) by matching the human protein database (*Homo sapiens*, *uniprot-proteome_UP000005640.fasta*) and label free quantification of identified proteins was then performed as previously described.[21]

Protein hit filtering methods and significance

Experiments were replicated three times to assess reproducibility. Only proteins detected in three replicates (LFQ intensity > 0) were used for further analyses. LFQ intensity was used to approximate the relative protein abundance between the different types of nGOs, while intensity was used to represent the protein abundance for each type of nGO individually. A student's t-test was used to evaluate the significance of differences observed across the three independent replicates between nGO-PEG and nGO-PEtOx, and p-values < 0.05 were considered significant.

Protein informatics and network annotation

The MaxQuant output (protein_groups.csv) was filtered to remove all proteins with less than one unique peptide, and with zero values for LFQ intensity across the nGO-PEG and nGO-PEtOx experiments. Additional processing included log_2 transforms, means, standard deviations, LFQ ratios and t-tests. Protein sequences and annotations were extracted from the UniProt Human proteome (*uniprot-proteome_UP000005640.fasta*) by matching to protein identifiers in the filtered protein list. For the matched set of protein sequences, the grand average of hydropathy (GRAVY), isoelectric point (pI), and molecular weight (MW) were calculated. To produce a contextual human plasma proteome background, a non-glycosylated PeptideAtlas build was downloaded (*20170801-063918 –* to recall the results used, visit this link db.systemsbiology.net/sbeams/cgi/shortURL?key=cga2kglb – provided in supplementary material) and both the protein identifiers and sequences were extracted from the UniProt *.fasta file: GRAVY, pI and MW were calculated for these sequences (*as above*) and used as a background proteome. The complete R data import, processing and presentation code, as well as session information that includes computer, software and package versions, are detailed in supplementary information.[43, 44] Proteins were submitted for matching of uniprot identifiers to STRING identifiers (http://www.uniprot.org/uploadlists/). The subset of matched STRING identifiers were used for protein network analysis with a whole genome background using the online resource STRING (v10.5, string-DB.org/).[45] Interactions were defined by *database* and *experimentally determined* sources at a confidence interaction score of 0.7 (medium). No additional

possible interactors were added. Color highlighting was used to emphasize gene ontology (GO) terms enriched by the analysis, and color halos were used to indicate PEG- or PEtOx-enrichment. All plots were formatted further in InkScape (inkscape.org) or used directly.

HEK 293 cell viability assay

For the cell viability assay, nGO, nGO-PEG, nGO-PEtOx, PEG and PEtOx of different concentrations were first diluted in PBS to make up stock suspensions. A black/clear bottom Costar 96 well plate was coated with poly-L-lysine for 20 min at 37 °C and then washed 3× in DPBS to promote cell adhesion. Human embryonic kidney 293 (HEK 293 from ATCC) cells, one of the most commonly used cell models for nanotoxicity studies, were seeded at a density of 10,000 cells per well in 200 μL complete DMEM (Sigma, 10% FBS) and incubated overnight at 37 °C and 5% CO_2. Media was then refreshed and samples were added into the wells to make up the final tested concentrations. After treatment for 24 h, media was aspirated and wells were washed 3× in DPBS and then 100 μL pre-diluted (1 in 10 dilution) alamarBlue in media was added to each well. The plate was returned to incubator for 3.5 h before endpoint fluorescence was read on a Flexstation 3 plate reader (Molecular Devices) with excitation at 544 nm and emission at 590 nm. Percentage cell viability was determined as comparative fluorescence intensity to untreated cells after deduction of background fluorescence. Experiments were conducted in triplicate.

Red blood cell (RBC) haemolysis assay

The haemolysis assay was slightly modified according to previously published protocols.[46, 47] Briefly, freshly drawn healthy human donor blood (50 μL) was added to 1.5 mL Eppendorf tubes, containing approximately 2.5×10^8 RBCs. The blood was washed 5× in PBS (pellets centrifuged down using 500 *g* and supernatant removed) and then diluted in PBS. Then nGO, nGO-PEG, nGO-PEtOx with and without plasma protein corona as well as PEG and PEtOx polymers diluted in PBS were added to the tubes containing RBCs to make final concentrations of 100, 50, 20, 10 and 5 μg/mL and incubated at 37 °C for 2 h. There were no other assay components to interfere with the nGO derivatives interacting

with the cells. Following incubation, supernatants (100 μL) of the tubes were transferred to a clear bottom Costar 96 well plate and the absorbance was read on a Flexstation 3 plate reader (Molecular Devices) at 570 nm (haemoglobin released from haemolytic RBCs). RBCs treated with Milli-Q water and PBS alone were used as positive and negative control. Percentage haemolysis was calculated from absorbance measured after normalization. Samples containing RBCs (RBCs were fixed by 2.5 % paraformaldehyde and PBS was replaced by ethanol using gradient dilution from 20% to 100% of ethanol) were mounted on SEM specimen stubs coated with carbon tapes and images were taken using an ORION NanoFab scanning helium ion microscope.

RESULTS AND DISCUSSION

PEG and PEtOx with primary amine end groups (MW ~2000 Da, determined by NMR; Figure S1, Electronic Supplementary Information or ESI) were successfully synthesized using a two-step reaction according to published protocols (Scheme 1).[40, 41] Size exclusion chromatography (SEC) revealed mono-modal traces with narrow molecular weight distributions for both polymers (Đ, PEtOx = 1.06, PEG = 1.06, Figure S1). nGO was first functionalized by carboxylation, and then the two types of polymers were grafted onto the surface of nGO by N-(3-dimethylaminopropyl)-N'-ethylcarbodiimide hydrochloride (EDC) coupling.[48, 49] The average lateral dimensions (50×100 nm) of bare nGO (carboxylated before polymer grafting) and PEG- and PEtOx-grafted nGO were estimated from TEM images (Figure 1). Successful grafting of the polymers was first confirmed using ATR-FTIR and energy-dispersive X-ray spectroscopy (EDX) (Figures S2 and S3). ATR-FTIR detected the characteristic chemical bond peaks associated with nGO (e.g. OH stretch at 3,340 cm^{-1}) and their attached polymers (e.g., ether bond at 1,100 cm^{-1} for PEG and amide C=O stretch at 1,630 cm^{-1} for PEtOx). Although not definitively quantitative, EDX identified nitrogen from the amide bond linking nGO to the polymers (apart from the nitrogen from PEtOx) which also confirmed successful grafting. To precisely quantify the amount of polymers grafted, TGA was performed on the three types of nGO. The grafting density of the polymers was estimated by the percentage weight losses

obtained from TGA (Figure S4), where PEG (decomposed from ~307 to 434 °C) and PEtOx (decomposed from ~321 to 473 °C) occupied 31.4% and 29.5% of the total mass of nGO-PEG and nGO-PEtOx, respectively. The hydrodynamic sizes (z-average sizes) and zeta potentials of bare nGO, nGO-PEG and nGO-PEtOx were determined by dynamic light scattering (DLS) (Table 1). The hydrodynamic sizes of the PEG- and PEtOx-grafted nGO sheets (318.5 and 291.2 nm, respectively) were smaller than bare nGO (364.2 nm), indicating improved suspension due to surface functionalization. No large agglomerates were observed for the samples, according to the hydrodynamic z-averages of the nGO derivatives measured by DLS. The nGO, nGO-PEG and nGO-PEtOx were relatively monodisperse, with PDI < 0.3. The zeta potentials ranged from -40.8 mV for nGO to -31.4 mV for nGO-PEG and -25.2 mV for nGO-PEtOx, indicating good colloidal suspendibility.

Raman spectra revealed the characteristic G and D bands of all three types of nGO, with the G band red-shifted by ~6 and 7 cm^{-1} in PEGylated and PEtOxylated nGO spectra, respectively. When bare nGO, nGO-PEG and nGO-PEtOx were coated with plasma proteins, all the G bands further red-shifted by ~8, 6 and 7 cm^{-1}, respectively (Figure S5). To determine the composition of plasma proteins in the nGO coronas, a proteomic study was undertaken using label-free LC-MS/MS analysis. This enabled an in-depth investigation of the antifouling capacities of PEG- and PEtOx-grafted nGO, as compared to bare nGO, which was used as a control. Compared to bare nGO, both nGO-PEG and nGO-PEtOx bound much smaller amounts of total protein which can be clearly observed from the heatmap of a global comparison of the protein abundance levels (Figure S6). Although this confirmed the strong antifouling capacities of both PEG and PEtOx, the polymers did bind distinct proteins. The LC-MS/MS analysis identified 129 proteins associated with all three types of nGO and 37 unique proteins associated with either two or one type of nGO, obtained from three replicate experiments.

The 10 most abundant proteins for bare nGO, nGO-PEG and nGO-PEtOx coronas, as well as for plasma, are listed in Table 2. As expected, the abundance distributions of corona proteins associated

with the three nGO nanomaterials were different from that of the plasma. For example, serum albumin [gene name: *ALB* (uniprot identifier: P02768)], the most abundant protein in plasma, was the most abundant for bare nGO, eighth for nGO-PEG and not in the top 10 for nGO-PEtOx. Overall, PEG and PEtOx displayed very comparable binding preferences for the top 10 most abundant proteins, which supports the viability of PEtOx as a surface modifier for nano-systems. Key differences in the top 10 include the presence of apolipoprotein A-I [*APOA1* (P02647)] and serum albumin [*ALB* (P02768)] on nGO-PEG as well as complement C3 [*C3* (P01024)] on nGO-PEtOx.

To more closely evaluate differences in corona composition, unique protein binders were considered. The Venn diagram in Figure 2a highlights the numbers of proteins which were bound to one, two, or all three nGO types. A total of 17 proteins were unique to one type of nGO, out of which 11 were unique to bare nGO (Table 3, Figure 2a). Of the unique nGO-associated proteins, it is worth noting that many were immunoglobulins, which suggests that rapid blood clearance of nGO opsonized by antibodies may occur without a stealth polymer coating: detected immunoglobulins included *IGKV2-29* (A2NJV5), *IGHV6-1* (A0A0B4J1U7), *IGKV2-28* (A0A075B6P5), *IGLV1-40* (P01703) and *IGLV3-10* (A0A075B6K4) (Table 3).

Focusing on relative enrichment of proteins in the evaluated coronas between nGO-PEG and nGO-PEtOx revealed significant disparities among a number of proteins. The $\log_2$ normalized abundance ratio of nGO-PEG versus nGO-PEtOx are presented in Figure 2b, with arbitrary ratio thresholds set to 0.5 and 2.0. Overall, 15 and 8 proteins were found to be significantly enriched in the corona of PEG- and PEtOx-grafted nGO, respectively. Angiogenin [*ANG*, P03950] exhibited a fold change of 0.08, or the highest relative affinity for nGO-PEtOx, while vitamin K-dependent protein S [*PROS1* (P07225)] and transthyretin [*TTR* (P02766)] both exhibited mean fold differences of 6.71, the highest relative affinities for nGO-PEG. Some additional proteins enriched on nGO-PEG included multiple apolipoproteins − *APOA1* (P02647)*, APOA2* (V9GYM3)*, APOC1* (K7ERI9)*, APOA4* (P06727)*, APOH* (P02749)*, CLU* (P10909) and the complement proteins *CFB* (B4E1Z4), *CFI* (G3XAM2) and

C4BPA (P04003) (Table 4). In contrast, nGO-PEtOx enriched pro-angiogenic protein [*ANG* (P03950)], structural protein [*FBLN1* (B1AHL2)], acute phase proteins [*SAA1* (P0DJI8)*, SAA2-A4* (A0A096LPE2)] as well as complement components [*C4B* (P0C0L5)*, C8B* (F5GY80), *C1QC* (P02747)], making this particle enrichment profile quite distinct from nGO-PEG (Figure 2b, Table 4).

A qualitative assessment of calculated − primary sequence specific − characteristics of the corona proteins was also undertaken, including GRAVY, pI and MW. Figure 3 shows the GRAVY/pI distributions (MW/pI in Figure S7) for the quantified proteins, with point color representing the fold-change bin to which the $\log_2$-normalized ratios of mean PEG: mean PEtOx LFQ intensity value belong. These points were overlaid onto a contextualizing non-glycosylated human plasma protein background from *PeptideAtlas*. Here, it was assumed that the matched database sequence for the identified protein was identical to that of the nGO-associated protein sequence. The quantified proteins appeared to cluster with the general protein characteristics of the plasma background, with no major trends apparent. A slight but visually discernible trend included nGO-PEG enriched proteins exhibiting more acidic pI values, as compared to nGO-PEtOx. Eight of the top ten nGO-PEG enriched proteins (*PROS1, TTR, CLU, APOA1, APOC1, SERPINF1, B2M and APOA4*) have pI values in the range of 5.0-6.5, and the outliers were *C4BPA* and *APOA2*. No such trend was apparent for nGO-PEtOx enriched proteins.

To further contextualize the relative composition differences of these coronas, a protein network analysis was performed using the STRING resource (string-db.org). This allowed identification of network associations and associated GO terms. Figure 4 highlights the resulting protein network and the colors of the nodes (proteins) indicate enrichment for a particular GO term. *Complement activation* is highlighted in red as an enriched biological process (BP), *enzyme regulator activity* is in blue as an enriched GO molecular function (MF), and finally *complement and coagulation cascades* is in green as an enriched Kyoto Encyclopedia of Genes and Genomes (KEGG) pathway. The halos

in Figure 4 indicate those protein significantly regulated (see red protein ratios in Figure 2b), which were enriched on nGO-PEG (yellow) or nGO-PEtOx (black). Both PEG and PEtOx functionalized nGO bound complement components that are part of the coagulation cascade (Figure 4). The implication here is that both nanomaterials may be similarly susceptible to reduced biocirculation. Overall, the split enrichment of different complement and coagulation components by nGO-PEG and nGO-PEtOx, and the over-representation of apolipoproteins by nGO-PEG could have profound implications *in vivo* following administration of nGO-based nanomedicines, which should be studied in the future.

Figure 5 shows a comparison of top 10 abundant corona proteins associated with PEGylated and PEtOxylated nGO (incubated in human plasma) in the present study with that of POS NPs (incubated in fetal calf serum) extracted from the literature.[31] Interestingly, completely different sets of proteins were observed between the two different NP cores, even if the surface modifications were similar. Serum albumin which is a globular protein is the most abundant corona protein for the spherical POS NPs, whereas rod-like fibrinogen represents the highest corona protein level for the 2D nanomaterial nGO. This comparison, though of limited validity due to the different experimental conditions employed (incubation time, biological media, corona extraction methodologies, etc.), still indicates that the shape of NP cores is likely as important as NP surface coating in determining protein binding and corona formation.

In addition to the proteomic study, HEK 293 cell viability was 51.3±7.1% when exposed to 100 µg/mL of bare nGO (Figure 6a). However, both PEG- and PEtOx-grafted nGO largely ameliorated the cell viability to above 80%. In contrast, no obvious toxicity was observed for the three types of nGO or the polymers at 50 µg/mL or lower, which confirmed the good biocompatibility of nGO and, in particular, stealth polymer-grafted nGO. The RBC haemolysis assay further revealed that both nGO-PEG and nGO-PEtOx induced negligible damage to cell membranes, while the presence of protein coronas largely mitigated haemolysis induced by nGO, nGO-PEG and nGO-PEtOx at

concentrations up to 100 μg/mL (Figure 6b). Images from helium ion microscopy clearly illustrated haemolytic damage of RBCs induced by bare nGO (Figure 6d), and the absence of obvious damage in the other samples through the protection of plasma proteins (Figure 6g) or stealth polymers PEG and PEtOx (Figures 6e,f,h,i).

CONCLUSION

We have characterized and compared human plasma corona proteome associations of linear PEG- and PEtOx-grafted nGO sheets and augmented the examination with viability and haemolysis assays. Although ample similarities have been observed for the strong antifouling capacities of both nGO-PEG and nGO-PEtOx, there were notable differences in the protein corona compositions of the two types of nanomaterials. Specifically, nGO-PEG enriched a number of apolipoproteins, suggesting its higher affinity for association with lipophilic environments such as cell membranes. In contrast, nGO-PEtOx displayed a preference for enriching pro-angiogenic, structural binding and acute phase proteins, among others. In addition, PEG- and PEtOx-grafted nGO displayed enrichment of different complement proteins (*CFB, CFI, C4BPA* for nGO-PEG, while *C4B, C8B, C1QC* for nGO-PEtOx*)* indicating comparable phagocytic recognition. Overall, nGO-PEG and nGO-PEtOx showed a very similar antifouling capacity, although neither was able to completely prevent protein binding. Both nGO-PEG and nGO-PEtOx were biocompatible, as corroborated by the HEK 293 cell viability and RBC haemolysis assays. In connection with existing literature, this study has further implicated the role of the NP substrate in determining their surface protein enrichment. Together, this study has provided a first comprehensive comparison on the stealth capacities and corona composition of PEtOx versus PEG against the human plasma proteome and, in light of the advantages of PEtOx over PEG in chemical adaptability, low viscosity, clearance, and non-immunogenicity,[28] should prove valuable for the continued development of nanomedicine and bionanotechnology. Towards that end, more in-depth protein corona studies on POx-grafted particles and surfaces will be necessary in the near future to gain further insights on the biological effects of the stealth polymer.

Electronic Supplementary Information (ESI): Nanomaterials characterizations, heatmap of protein abundance levels, MW vs. pI of the proteins associated with the nanomaterials, and R script.

AUTHOR CONTRIBUTIONS

PCK, KK and TPD conceived the study. MW, TB, HY and KK performed the materials synthesis and characterisations. MW, GS and DJC performed the LC-MS assays and OJRG conducted proteomic data analysis and informatics. IJ, MW, HGK conducted the haemolysis assay. MW, PCK, OJRG and KK wrote the paper.

CONFLICT OF INTEREST

The authors declare no conflict of interest.

FIGURES
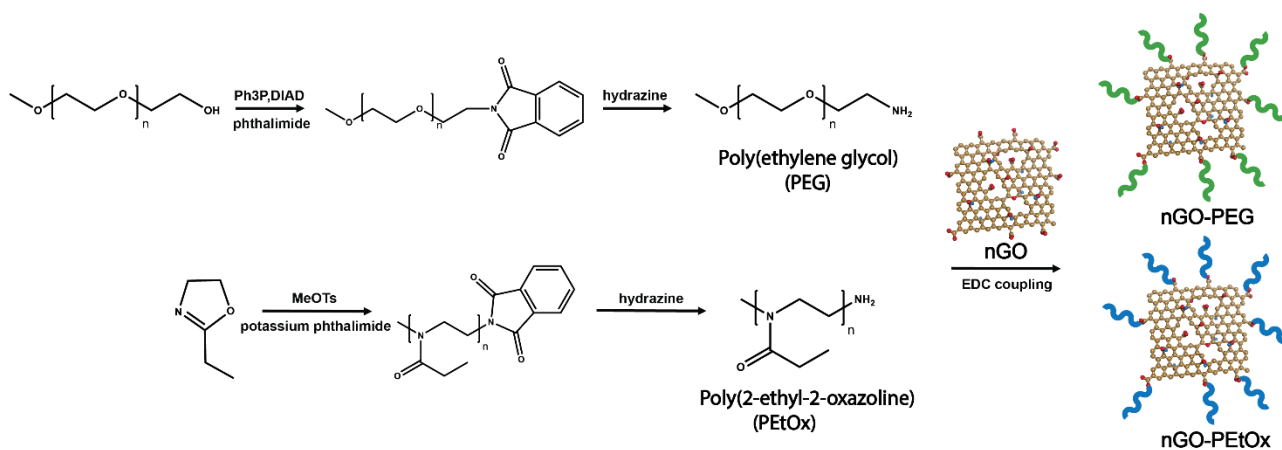
Scheme 1. Synthesis of PEG and PEtOx and their grafting onto nGO (carbon: brown, oxygen: red, hydrogen: blue).
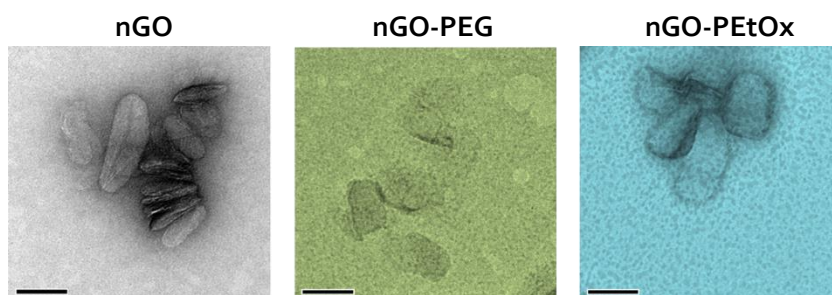
Figure 1. TEM images of the three types of nGO sheets. Scale bars: 100 nm. Pseudo-colors for nGO-PEG and nGO-PEtOx.

(a)
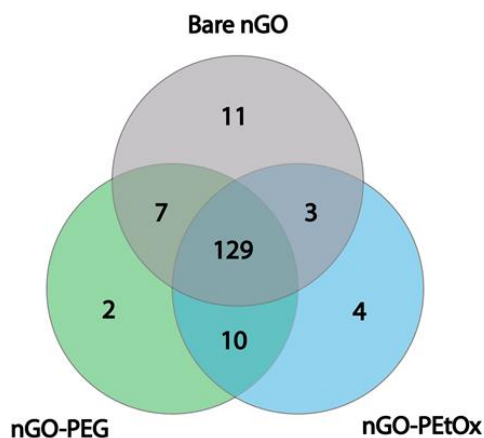
(b)
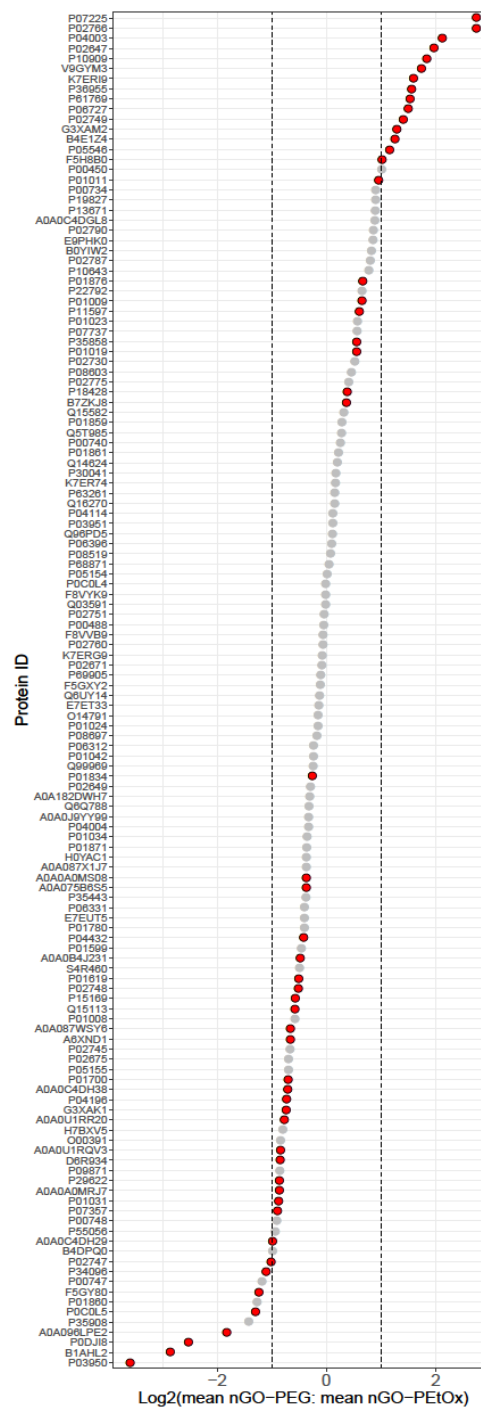
Figure 2. (a) Venn diagram representing the common and unique proteins associated with three nGO surface chemistries: bare (nGO), PEG (nGO-PEG) and POx (nGO-PEtOx). The result was acquired following 24 h incubation with human plasma proteins. (b) Log_2 normalized protein abundance ratio plotted against log_2 normalized mean (N = 3) nGO-PEG:nGO-PEtOx protein LFQ intensity values with arbitrary ratio cut-offs of 0.5 and 2 (dashed black lines). Red dots represent coronal proteins that are significantly different in abundance (t-test mean LFQ intensity values) between nGO-PEG and nGO-PEtOx. Proteins are identified by their respective unique identifiers.
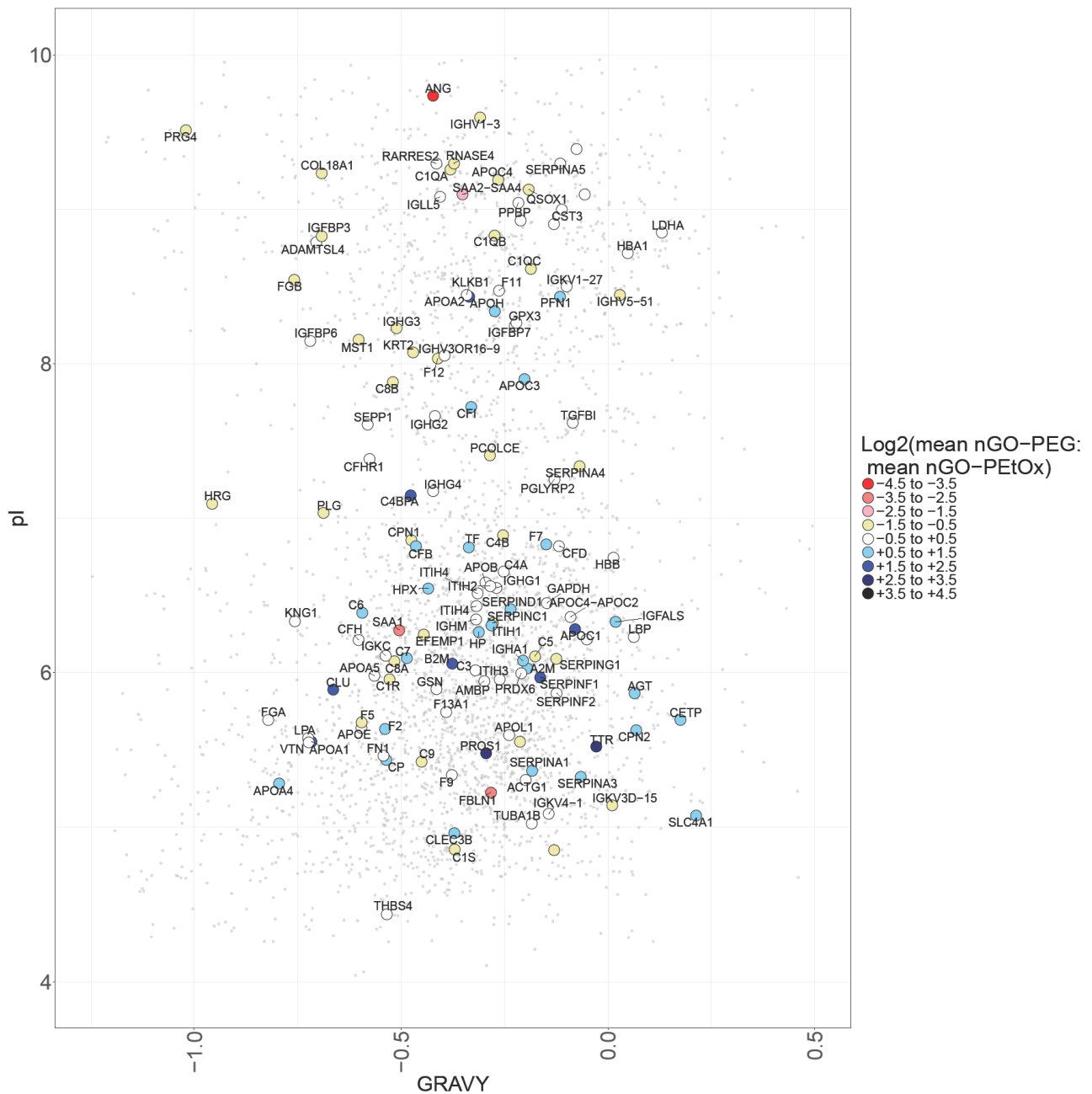
Figure 3. The pI vs GRAVY distributions for corona proteins on nGO-PEG and -PEtOx are presented. Spot color indicates the abundance bin to which each protein belongs – based on $\log_2$ normalized ratio of mean LFQ (nGO-PEG):mean LFQ (nGO-PEtOx). The grey dots represent a non-glycosylated plasma background from Peptide Atlas (*20170801-063918*) without abundance information. Proteins are annotated with their respective gene names for clarity. GRAVY and pI ranges were manually selected.

Figure 4. Protein network analysis using the STRING resource (v10.5, string-db.org). The network was generated from 82 matched gene name entries (N = 134 total), using *experiments* and *databases* as active interaction sources, a minimum required interaction score of 0.7 (high confidence), no additional interactors and a whole genome background. Gene ontology (GO) annotations generated as part of the analysis were added, including *complement activation* in red (biological process [BP]), *enzyme regulator activity* in blue (molecular function [MF]) and *complement and coagulation cascades* in green (KEGG). Color halos indicate those proteins which were significantly different, determined by t-test of mean LFQ intensity values: PEG-enriched are yellow and PEtOx-enriched are black.

Figure 5. Comparison of top 10 most abundant corona proteins of PEGylated and PEtOxylated nGO and that of poly(organosiloxane) (POS) NPs from ref 31.
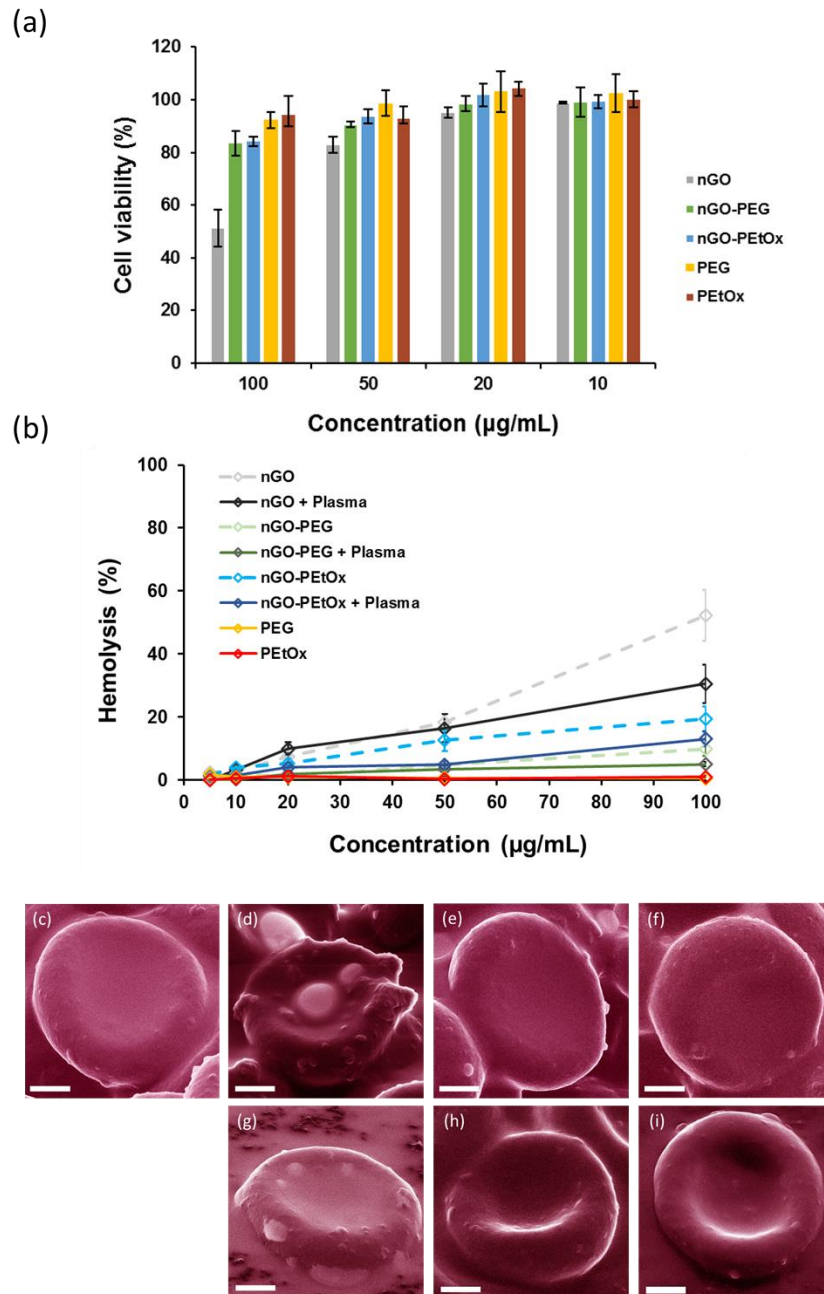
Figure 6. (a) Viability of HEK 293 cells determined using alamarBlue after treatment with different concentrations (100, 50, 20 and 10 μg/mL) of nGO, nGO-PEG, nGO-PEtOx, PEG polymer and PEtOx polymer for 24 h. Values were expressed as means ± SD (N = 3). (b) Haemolysis assay using red blood cells treated with different concentrations (100, 50, 20, 10 and 5 μg/mL) of nGO, nGO-PEG, nGO-PEtOx w/o plasma protein corona as well as PEG and PEtOx polymers for 2 h. Values were expressed as means ± SD (N = 3). Images of red blood cells alone (c) and red blood cells treated for 2 h with nGO (d), nGO-PEG (e) and nGO-PEtOx (f) (100 μg/mL) as well as nGO (g), nGO-PEG (h), nGO-PEtOx (i) with plasma protein coatings. Images acquired using a scanning helium ion microscope. Scale bars: 1 μm.

TABLES

Table 1. Zeta potentials and hydrodynamic sizes of the nGO sheets in Milli-Q water.

Nanomaterials	Zeta potential (mV)	Hydrodynamic size (nm)	PDI
nGO	-40.8 ± 0.6	364.2 ± 5.6	0.23 ± 0.01
nGO-PEG	-31.4 ± 0.5	318.5 ± 4.8	0.20 ± 0.01
nGO-PEtOx	-25.2 ± 0.5	291.2 ± 4.4	0.22 ± 0.01

Table 2. Top-10 most abundant proteins associated with each type of nGO.

No.	Bare nGO	nGO-PEG	nGO-PEtOx	Plasma
1	Serum albumin	Fibrinogen alpha chain	Fibrinogen alpha chain	Serum albumin
2	Fibrinogen gamma chain	Fibrinogen gamma chain	Fibrinogen beta chain	Ig heavy constant gamma 1
3	Complement C4-B	Fibrinogen beta chain	Fibrinogen gamma chain	Fibrinogen beta chain
4	Inter-alpha-trypsin inhibitor heavy chain H4	Inter-alpha-trypsin inhibitor heavy chain H4	Inter-alpha-trypsin inhibitor heavy chain H4	Complement C3
5	Ig heavy constant gamma 1	Ig heavy constant gamma 1	Ig heavy constant gamma 1	Serotransferrin
6	Fibrinogen alpha chain	Apolipoprotein A-I	Kininogen-1	Apolipoprotein A-I
7	Fibrinogen beta chain	Gelsolin	Gelsolin	Alpha-1-antitrypsin
8	Complement C3	Serum albumin	Complement C3	Fibrinogen alpha chain
9	Gelsolin	Kininogen-1	Vitronectin	Haptoglobin
10	Apolipoprotein B-100	Apolipoprotein B-100	Apolipoprotein B-100	Alpha-2-macroglobulin

Table 3. Proteins unique to the nGO coronas.

	Uniprot IDs	Gene names	Protein names
Bare nGO	A2NJV5	IGKV2-29	Immunoglobulin kappa variable 2-29
	A0A0B4J1U7	IGHV6-1	Immunoglobulin heavy variable 6-1
	A0A075B6P5	IGKV2-28	Immunoglobulin kappa variable 2-28
	P98160	HSPG2	Basement membrane-specific heparin sulfate proteoglycan core protein
	P06702	S100-A9	Protein S100-A9
	P01703	IGLV1-40	Immunoglobulin lambda variable 1-40
	Q14520	HABP2	Hyaluronan-binding protein 2
	P05109	S100A8	Protein S100-A8
	E5RH81	CA1	Carbonic anhydrase 1
	Q9NQ79	CRTAC1	Cartilage acidic protein 1
	A0A075B6K4	IGLV3-10	Immunoglobulin lambda variable 3-10
nGO-PEG	Q9UGM5	FETUB	Fetuin-B
	Q8WUA8	TSKU	Tsukushin
nGO-PEtOx	P48740	MASP1	Mannan-binding lectin serine protease 1
	P26572	MGAT1	Alpha-1,3-mannosyl-glycoprotein 2 beta-N-acetylglucosaminyltransferase
	Q15485	FCN2	Ficolin-2
	O15335	CHAD	Chondroadherin

Table 4. Protein abundance ratio of nGO-PEG versus nGO-PEtOx (less than 0.5 and greater than 2.0 is the fold difference threshold, and only proteins that are significantly different between nGO-PEG and nGO-PEtOx are listed).

| Uniprot IDs	Protein names (*Gene names*)	Mean abundance ratio	p value
P03950	Angiogenin (*ANG*)	0.08	0.02
B1AHL2	Fibulin-1 (*FBLN1*)	0.14	< 0.01
P0DJI8	Serum amyloid A-1 protein (*SAA1*)	0.17	0.02
A0A096LPE2	Serum amyloid A-4 protein (*SAA2-A4*)	0.28	< 0.01
P0C0L5	Complement C4-B (*C4B*)	0.41	< 0.01
F5GY80	Complement component C8 beta chain (*C8B*)	0.42	< 0.01
P34096	Ribonuclease 4 (*RNASE4*)	0.46	0.01
P02747	Complement C1q subcomponent subunit C (*C1QC*)	0.49	0.04
F5H8B0	Coagulation factor VII (*F7*)	2.02	< 0.01
P05546	Heparin cofactor 2 (*SERPIND1*)	2.23	0.02
B4E1Z4	Complement factor B (*CFB*)	2.38	0.01
G3XAM2	Complement factor I (*CFI*)	2.44	0.01
P02749	Apolipoprotein H (*APOH*)	2.64	0.01
P06727	Apolipoprotein A-IV (*APOA4*)	2.82	< 0.01
P61769	Beta-2-macroglobulin (*B2M*)	2.89	< 0.01
P36955	Pigment epithelium-derived factor (*SERPINF 1*)	2.94	< 0.01
K7ERI9	Apolipoprotein C-I (*APOC1*)	3.02	0.02
V9GYM3	Apolipoprotein A-II (*APOA2*)	3.34	< 0.01
P10909	Clusterin (*CLU*)	3.57	< 0.01
P02647	Apolipoprotein A-1 (*APOA1*)	3.91	< 0.01
P04003	C4b-binding protein alpha chain (*C4BPA*)	4.35	0.04
P02766	Transthyretin (*TTR*)	6.71	< 0.01
P07225	Vitamin K-dependent protein S (*PROS1*)	6.71	0.02

References

1. E. Blanco, H. Shen, M. Ferrari, *Nat. Biotechnol.* **2015**, *33*, 941.

2. G. Chen, I. Roy, C. Yang, P. N. Prasad, *Chem. Rev.* **2016**, *116*, 2826.

3. S. Schöttler, G. Becker, S. Winzen, T. Steinbach, K. Mohr, K. Landfester, V. Mailänder, F. R. Wurm, *Nat. Nanotechnol.* **2016**, *11*, 372.

4. T. Cedervall, I. Lynch, S. Lindman, T. Berggård, E. Thulin, H. Nilsson, K. A. Dawson, S. Linse, *Proc. Natl. Acad. Sci. USA* **2007**, *104*, 2050.

5. I. Lynch, K. A. Dawson, *Nano Today* **2008**, *3*, 40.

6. F. Ding, S. Radic, R. Chen, P. Chen, N. K. Geitner, J. M. Brown, P. C. Ke, *Nanoscale* **2013**, *5*, 9162.

7. J. H. Shannahan, J. M. Brown, R. Chen, P. C. Ke, X. Lai, S. Mitra, F. A. Witzmann, *Small* **2013**, *9*, 2171.

8. M. P. Monopoli, C. Aberg, A. Salvati, K. A. Dawson, *Nat. Nanotechnol.* **2012**, *7*, 779.

9. H. Amiri, L. Bordonali, A. Lascialfari, S. Wan, M. P. Monopoli, I. Lynch I, *Nanoscale* **2013**, *5*, 8656.

10. D. Song, J. Cui, H. Sun, T. H. Nguyen, S. Alcantara, R. De Rose, S. T. Kent, C. J. H. Porter, F. Caruso, *ACS Appl. Mater. Interfaces* **2017**, *9*, 33683.

11. M. Mahmoudi, I, Lynch, M. R. Ejtehadi, M. P. Monopoli, F. B. Bombelli, S. Laurent, *Chem. Rev.* **2011**, *111*, 5610.

12. P. C. Ke, S. Lin, W. J. Parak, T. P. Davis, F. Caruso, *ACS Nano* **2017**, *11*, 11773.

13. K. Knop, R. Hoogenboom, D. Fischer, U. S. Schubert, *Angew. Chem. Int. Ed.* **2010**, *49*, 6288.

14. H. Otsuka, Y. Nagasaki, K. Kataoka, *Adv. Drug Deliv. Rev.* **2003**, *55*, 403.

15. B. Pelaz, P. del Pino, P. Maffre, R. Hartmann, M. Gallego, S. Rivera-Fernández, J. M. de la Fuente, G. U. Nienhaus, *ACS Nano* **2015**, *9*, 6996.

16. C. D. Walkey, J. B. Olsen, H. Guo, A. Emili, W. C. W. Chan, *J. Am. Chem. Soc.* **2012**, *134*, 2139.

17. T. Ishida, H. Kiwada. *Biol. Pharm. Bull.* **2013**, *36*, 889.

18. S. Shah, T. Prematta, N. F. Adkinson, F. T. Ishmael, *J. Clin. Pharmacol.* **2013**, *53*, 352.

19. C. Fetsch, A. Grossmann, L. Holz, J. F. Nawroth, R. Luxenhofer, *Macromolecules* **2011**, *44*, 6746.

20. K. H. A. Lau, C. Ren, T. S. Sileika, S. H. Park, I. Szleifer, P. B. Messersmith, *Langmuir* **2012**, *28*, 16099.

21. M. Wang, G. Siddiqui, O. J. R. Gustafsson, A. Kakinen, I. Javed, N. H. Voelcker. D. J. Creek, P. C. Ke, T. P. Davis, *Small* **2017**, *13*, 1701528.

22. R. Hoogenboom, *Angew. Chem. Int. Ed.* **2009**, *48*, 7978.

23. E. Rossegger, V. Schenk, F. Wiesbrock, *Polymers* **2013**, *5*, 956.

24. K. Kempe, *Macromol. Chem. Phys*. **2017**, *218*, 1700021

25. B. Guillerm, S. Monge, V. Lapinte, J-J. Robin, *Macromol. Rapid Commun*. **2012**, *33*, 1600

26. R. Luxenhofer, Y. Han, A. Schulz, J. Tong, Z. He, A. V. Kabanov, R. Jordan, *Macromol. Rapid Commun*. **2012**, *33*, 1613

27. O. Sedlacek, B. D. Monnery, S. K. Filippov, R. Hoogenboom, M. Hruby, *Macromol. Rapid Commun*. **2012**, *33*, 1648

28. R. W. Moreadith, T. X. Viegas, M. D. Bentley, J. M. Harris, Z. Fang, K. Yoon, B. Dizman, R. Weimer, B. P. Rae, X. Li, C. Rader, D. Standaert, W. Olanow, *Eur. Polym. J*. **2017**, *88*, 524

29. K. Kempe, S. L. Ng, S. T. Gunawan, K. F. Noi, F. Caruso, *Adv. Funct. Mater.* **2014**, *24*, 6187

30. O. Koshkina, T. Lang, R. Thiermann, D. Docter, R. H. Stauber, C. Secker, H. Schlaad, S. Weidner, B. Mohr, M. Maskos, A. Bertin, *Langmuir* **2015**, *31*, 8873

31. O. Koshkina, D. Westmeier, T. Lang, C. Bantz, A. Hahlbrock, C. Würth, U. Resch-Genger, U. Braun, R. Thiermann, C. Weise, M. Eravci, B. Mohr, H. Schlaad, R. H. Stauber, D. Docter, A. Bertin, M. Maskos, *Macromol. Biosci*. **2016**, *16*, 1287

32. P. Wilson, P. C. Ke, T. P. Davis, K. Kempe, *Eur. Polym. J.* **2017**, *88*, 486

33. Y. Song, Y. Chen, L. Feng, J. Ren, X. Qu, *Chem. Commun.* **2011**, *47*, 4436.

34. C. H. Lu, H. H. Yang, C. L. Zhu, X. Chen, G. N. Chen, *Angew. Chem. Int. Ed.* **2009**, *48*, 4785.

35. X. Sun, Z. Liu, K. Welsher, J. T. Robinson, A. Goodwin, S. Zaric, H. Dai, *Nano Res.* **2008**, *1*, 203.

36. J. Luo, L. J. Cote, V. C. Tung, A. T. L. Tan, P. E. Goins, J. Wu, J. Huang, *J. Am. Chem. Soc.* **2010**, *132*, 17667.

37. Z. Liu, J. T. Robinson, X. Sun, H. Dai, *J. Am. Chem. Soc.* **2008**, *130*, 10876.

38. H. S. Jung, W. H. Kong, D. K. Sung, M. Y. Lee, S. E. Beack, D. H. Keum, K. S. Kim, S. H. Yun, S. K. Hahn, *ACS Nano* **2014**, *8*, 260.

39. X. Yang, X. Zhang, Y. Ma, Y. Huang, Y. Wang, Y. Chen, *J. Mater. Chem*. **2009**, *19*, 2710.

40. P. Mongondry, C. Bonnans-Plaisance, M. Jean, J. F. Tassin, *Macromol. Rapid Commun.* **2003**, *24*, 681.

41. L. Tauhardt, M. Frant, D. Pretzel, M. Hartlieb, C. Bucher, G. Hildebrand, B. Schröter, C. Weber, K. Kempe, M. Gottschaldt, K. Liefieth, U. S. Schubert, *J. Mater. Chem. B* **2014**, *2*, 4883

42. G. Siddiqui, A. Srivastava, A. S. Russell, D. J. Creek, *J. Infect. Dis.* **2017**, *215*, 1435.

43. R. C. Team, R Foundation for Statistical Computing, Vienna, Austria. **2017**:URL http://www.R-project.org/.

44. N. T. Gupta, J. A. Vander Heiden, M. Uduman, D. Gadala-Maria, G. Yaari, S. H. Kleinstein, *Bioinformatics* **2015**, *31*, 3356.

45. D. Szklarczyk, A. Franceschini, S. Wyder, K. Forslund, D. Heller, J. Huerta-Cepas, M. Simonovic, A. Roth, A. Santos, K. P. Tsafou, M. Kuhn, P. Bork, L. J. Jensen, C. von Mering, *Nucleic Acids Res*. **2015**, *43*, 447.

46. M. F. Sohail, H. S. Sarwar, I. Javed, A. Nadhman, S. Z. Hussain, H. Saeed, A. Raza, N. I. Bukhari, I. Hussain, G. Shahnaz, *Toxicol. Res*. **2017**, *6*, 814.

47. B. C. Evans, C. E. Nelson, S. S. Yu, K. R. Beavers, A. J. Kim, H. Li, H. M. Nelson, T. D. Giorgio, C. L. Duvall, *J. Vis. Exp*. **2013**, *73*, 50166.

48. H. R. Kim, A. Baek, I. J. Lee, D. E. Kim, *ACS Appl. Mater. Interfaces*. **2016**, *8*, 33521.

49. K. Yang, L. Feng, H. Hong, W. Cai, Z. Liu, *Nat. Protoc*. **2013**, *8*, 2392.

TABLE OF CONTENT
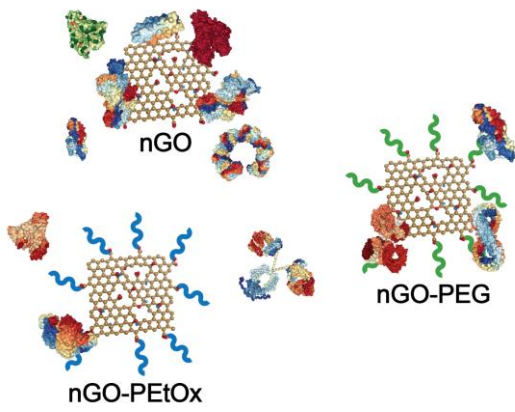
Human plasma proteome associations with nano-graphene oxide (nGO) sheets grafted with stealth polyethylene glycol (PEG) and poly(2-ethyl-2-oxazoline) (PEtOx)